

NISTIR 6030

**THIRTEENTH MEETING OF THE UJNR
PANEL ON FIRE RESEARCH AND SAFETY,
MARCH 13-20, 1996**

VOLUME 1

Kellie Ann Beall, Editor

June 1997
Building and Fire Research Laboratory
National Institute of Standards and Technology
Gaithersburg, MD 20899



U.S. Department of Commerce
William M. Daley, *Secretary*
Technology Administration
Gary R. Bachula, *Acting Under Secretary for Technology*
National Institute of Standards and Technology
Robert E. Hebner, *Acting Director*

Mathematical Modeling for Building Fire

Masahiro Morita

Department of Applied Mathematics,
Faculty of Science,
Science University of Tokyo

1-3 Kagurazaka, Shinjuku-ku,
Tokyo 162, JAPAN

ABSTRACT

Theoretical and experimental numerical analysis have proposed the capable of being executed computational finite difference method for fire induced natural convective heat flow using the viscous heat conductive compressible fluid with $K-\epsilon$ model in the fire compartment. Because two-point upwind difference scheme give the numerical viscosity, the computational results are different from the approximate solutions at the large velocity. The practical stability and the truncation errors for computing finite difference equations approximating fire governing equations have been introduced by theoretical numerical analysis. The sensitivities of numerical solutions have been evaluated by the theoretical and experimental numerical analysis. As the results of numerical experiments we proposed that the reasonable time interval and space mesh size are chosen considering the CPU time. Furthermore we have introduced the Re^* for the equation of motion or Pe^* for the equation of energy. We proposed that the values of Re^* and Pe^* indicate the trust in the approximate solutions in consequence of the numerical experiments.

1. Introduction

The numerical computations of a natural convective flow have been studied mainly in fluid dynamics [1]. In applied mathematics the theoretical and numerical analysis of Navier-Stokes (N-S) type equations have been investigated [2]. Ladyzhenskaya [2] proposed that the unique solution and the existence of analytical solution of N-S equation for the incompressible fluid flow are not guaranteed in high Reynolds number and only guaranteed at small Re number (less than about 100) at the initial and boundary conditions. The mathematical analysis for the compressible fluid flow does not be reported yet. None the less, the computer simulations for the field model applied to the fire phenomena have been reported by Hasemi [3]. However it is necessary to investigate the methods of numerical solution of the non-linear parabolic partial difference equations which are the basic governing fire equations.

Because most workers using numerical methods for the convection terms in the governing equations have adopted two-point upwind difference scheme, the computational results

do not give us the approximate solution because numerical viscosity is left out of consideration. Furthermore there is need to know how the truncation errors are dependence upon the time and space meshes in a fire problem influence the numerical solution.

In this paper, we have conducted calculations with several numerical computational finite difference methods for fire induced heat flow in the fire compartment using viscous heat-conductive compressible fluid (K- ϵ model) and have made a comparison with the computational results. Since numerical experiments are a difficult computational problem requiring considerable computer power, the problem was tackled using a super computer. We have also investigated the sensitivities of the numerical solutions with the time and space meshes by using numerical experiments, and investigated the stabilities of computational scheme.

2. Governing Equation

Fire induced heat flow of the growth and spread fire must be represented the compressible viscous fluid flow because of high temperature. However the heat flow of the smoldering fire is enough to represent the incompressible viscous fluid flow.

Mathematical field modeling for the heat flow represents two methods. Lagrange method is adopted that heat flow is treated by the moving fluid particles. It can be expressive of the appearance of the induced fluid flow. On the other hand, Euler method means that the heat flow is presented each flow pattern in a moment of fire. Euler method is in general used because of easier treatment than Lagrange method. The fire field model is important to model the turbulence for the fire induced heat flow with flow properties such as flame, plume and jet stream which are described maximum Reynolds number, maximum Prandtl number and Grashof number etc. of heat flow by experiments. There are two kinds of equations which are the dimensional equations and nondimensional equation. Until now the nondimensional equation is used for the fire simulational equation. This is never the best model because the nondimensional mesh size is depend upon the size of fire domain and is not represent the real size. However the nondimensional mesh size and the eddy length for the turbulence should have a close connection with each other.

The classification of numerical methods for turbulence of Navie-Stokes type equations follows:

(1) Direct method

(2) Average method

(2-1) Time average method

(2-1-1) Integral method

(i) Entrainment method

(2-1-2) Differential method

(2-1-2-1) Turbulence viscous model

• 0-equation model

(i) Mixing length model

(ii) Cebeci-Smith model

- 2-equation model
 - (i) $K - \epsilon$ model
- (2-1-2-2) Stress equation model
 - Bradshaw's 1-equation model
 - 3-equation model
- (2-2) Space average method
 - (i) Large Eddy Simulation (LES) model
- (2-3) Ensemble average method

Let us consider a series of the governing equations of the turbulent natural convection by using turbulent viscous transport model which is mathematically obtained by Reynolds decomposition in a fire compartment [3]. The well known field equations governing the thermophysical and thermochemical dynamics, and heat/mass transfer of a turbulent fluid are described, in principle, by the following set using Cartesian coordinate system.

2.1. Equation of continuity

$$\frac{\partial \bar{\rho}}{\partial t} + \frac{\partial \overline{\rho u_j}}{\partial x_j} = 0$$

or

$$\frac{\partial^2 \bar{P}}{\partial x_i^2} = \frac{\partial^2 \bar{\rho}}{\partial t^2} + \frac{\partial^2}{\partial x_i \partial x_j} \left\{ \bar{\tau}_{ij} + K \left(\frac{\partial \overline{\rho u_j}}{\partial x_i} + \frac{\partial \overline{\rho u_i}}{\partial x_j} \right) - \bar{\rho} \bar{u}_i \bar{u}_j \right\} - g \frac{\partial \bar{\rho}}{\partial x_2}$$

2.2. Equation of Motion

$$\frac{\partial \overline{\rho u_i}}{\partial t} + \frac{\partial \overline{\rho u_i u_j}}{\partial x_j} = - \frac{\partial \bar{P}}{\partial x_i} + \frac{\partial}{\partial x_j} \left\{ \bar{\tau}_{ij} + K \left(\frac{\partial \overline{\rho u_j}}{\partial x_i} + \frac{\partial \overline{\rho u_i}}{\partial x_j} \right) \right\} - \delta_{i2} \bar{\rho} g$$

2.3. Equation of energy

$$\frac{\partial \bar{\rho} \bar{h}}{\partial t} + \frac{\partial \overline{\rho h u_j}}{\partial x_j} = \frac{\partial}{\partial x_j} \left(\lambda_\theta \frac{\partial \bar{\theta}}{\partial x_j} + \bar{\rho} K \frac{\partial \bar{h}}{\partial x_j} \right) + \bar{Q}$$

$$\bar{h} = c_p \bar{\theta}$$

2.4. Equation of state

$$\bar{P} = \bar{\rho} R \bar{\theta}$$

2.5. Transport equation of turbulent energy

$$\frac{\partial \bar{\rho} \bar{q}}{\partial t} + \frac{\partial \overline{\rho q u_j}}{\partial x_j} = \frac{\partial}{\partial x_j} \left(\bar{\rho} K \frac{\partial \bar{q}}{\partial x_j} \right) + \mu \frac{\partial^2 \bar{q}}{\partial x_j^2} + g K \frac{\partial \bar{\rho}}{\partial x_2} - \bar{\rho} \bar{\epsilon}$$

$$+ K \frac{\partial \bar{u}_i}{\partial x_j} \left(\frac{\partial \overline{\rho u_j}}{\partial x_i} + \frac{\partial \overline{\rho u_i}}{\partial x_j} \right)$$

2.6 Eddy viscosity and energy decay rate

$$\begin{cases} K = c\bar{q}^2/\bar{\epsilon} \\ \bar{\epsilon} = c\bar{q}^3/l \end{cases}$$

Where $\bar{\rho}$ is density of fluid; x and y are spatial coordinate, horizontal and vertical direction; \bar{u} and \bar{v} are velocity, x - and y - direction; t is time; K is eddy viscosity coefficient; δ is Kronecker delta; g is acceleration of gravity; μ is dynamic viscosity; c_p is heat capacity; $\bar{\theta}$ is temperature; \bar{q} is turbulent energy; $\bar{\epsilon}$ is energy decay rate; λ_θ is thermal conductivity; \bar{h} is enthalpy; \bar{P} is pressure; \bar{Q} is generation of energy; l is Prandtl's length; R is gas constant; $\bar{\tau}$ is viscosity stress.

3. Numerical Computaional Method

We have only discussed the equation of energy, which is the non-linear parabolic 2nd order partial differential equation, in the governing equation because the other equations will be able to deal with the same manner. The energy equation is represented by using rectangular coordinate system; x , y and t for reason of simplifying. The velocities, x - and y -direction, are denoted \bar{u} and \bar{v} respectively. The energy equation is transformed by Reynolds stress [3] as follows;

3.1 Partial differential equation

$$\begin{aligned} \frac{\partial \bar{\theta}}{\partial t} + \bar{u} \frac{\partial \bar{\theta}}{\partial x} + \bar{v} \frac{\partial \bar{\theta}}{\partial y} &= \left(\frac{\lambda_\theta}{\bar{\rho} c_p} + K \right) \left\{ \frac{\partial^2 \bar{\theta}}{\partial x^2} + \frac{\partial^2 \bar{\theta}}{\partial y^2} \right\} \\ &+ \left\{ 2 \frac{K}{\bar{\rho}} \frac{\partial \bar{\rho}}{\partial x} + \frac{\partial K}{\partial x} \right\} \frac{\partial \bar{\theta}}{\partial x} + \left\{ 2 \frac{K}{\bar{\rho}} \frac{\partial \bar{\rho}}{\partial y} + \frac{\partial K}{\partial y} \right\} \frac{\partial \bar{\theta}}{\partial y} \end{aligned}$$

where no generation of internal heat in the equation of energy is adapted $\bar{Q} = 0$.

3.2. Finite difference approximation

As the analytical solutions of fire governing equations are not given yet, the above partial differential equation is transformed to discrete equations by Taylor expansion method etc. For the purpose of obtaining the approximate solution of the energy equation, let $\Delta x, \Delta y$ and Δt be small increments of variables x , y and t ; where $\Delta x = L/I$ and $\Delta y = H/J$, I and J being integers, and L and H being length and height of the domain respectively. The set of point in x, y, t -plane given by $x = i\Delta x$, $y = j\Delta y$ and $t = n\Delta t$; where $i = 0, 1, 2, \dots, I$, $j = 0, 1, 2, \dots, J$ and $n = 0, 1, 2, \dots$; is called a grid whose mesh size is determined by Δx , Δy and Δt . The approximation to $\bar{\theta}(i\Delta x, j\Delta y, n\Delta t)$ is denoted by θ_{ij}^n . In the same way, $\bar{u}(i\Delta x, j\Delta y, n\Delta t)$, $\bar{v}(i\Delta x, j\Delta y, n\Delta t)$, and $\bar{\rho}(i\Delta x, j\Delta y, n\Delta t)$, are denoted by u_{ij}^n , v_{ij}^n and ρ_{ij}^n , respectively. The finite difference equation [4] approximating

the energy equation is obtained

$$\begin{aligned} \frac{\theta_{ij}^{n+1} - \theta_{ij}^n}{\Delta t} + u_{ij}^m \left[\frac{\partial \theta}{\partial x} \right]_{ij}^k &= \left[\sigma_{ij}^m + K_{ij}^m \right] \left\{ \frac{\theta_{i+1j}^k - 2\theta_{ij}^k + \theta_{i-1j}^k}{\Delta x^2} + \frac{\theta_{ij+1}^k - 2\theta_{ij}^k + \theta_{ij-1}^k}{\Delta y^2} \right\} \\ &+ \left\{ \frac{K_{ij}^m}{\rho_{ij}^m} \frac{\rho_{i+1j}^m - \rho_{i-1j}^m}{\Delta x} + \frac{K_{i+1j}^m - K_{i-1j}^m}{2\Delta x} \right\} \frac{\theta_{i+1j}^k - \theta_{i-1j}^k}{2\Delta x} \\ &+ \left\{ \frac{K_{ij}^m}{\rho_{ij}^m} \frac{\rho_{ij+1}^m - \rho_{ij-1}^m}{\Delta y} + \frac{K_{ij+1}^m - K_{ij-1}^m}{2\Delta y} \right\} \frac{\theta_{ij+1}^k - \theta_{ij-1}^k}{2\Delta y} \end{aligned}$$

where

$$\begin{cases} \sigma_{ij}^m = \frac{\lambda_\theta}{\rho_{ij}^m c_p} \\ k = \begin{cases} n & \text{explicit scheme} \\ n+1 & \text{implicit scheme} \end{cases} \\ m = \begin{cases} n & \text{decoupled method} \\ n+1 & \text{coupled method} \end{cases} \end{cases}$$

The coupled method is exactly presented the original continuous fundamental equations. However as this method is more complicate for computaions and is difficult to have the computaional stability, it is not general used. Furthermore the computational results of coupled method are almost same values of those decoupled method. The decoupled method is used in our system for above reason. The time derivative term is approximated with two-point backward implicit ($k = n + 1$) time difference scheme. The diffusion terms and first order derivative terms are approximated with five-point or three-point central space difference scheme, respectively. The convection terms $u_{ij}^n \left[\frac{\partial \theta}{\partial x} \right]_{ij}^k$ and $v_{ij}^n \left[\frac{\partial \theta}{\partial y} \right]_{ij}^k$, which are represented by $a \left[\frac{\partial f}{\partial h} \right]_l$, are approximated with following scheme:

3.2.1. Central difference scheme

$$a \left[\frac{\partial f}{\partial h} \right]_l = \frac{f_{l+1} - f_{l-1}}{2\Delta h}$$

3.2.2 Two-point upwind difference scheme

$$a \left[\frac{\partial f}{\partial h} \right]_l = \begin{cases} a \frac{f_l - f_{l-1}}{\Delta h} & \text{if } a \geq 0 \\ a \frac{f_{l+1} - f_l}{\Delta h} & \text{if } a < 0 \end{cases}$$

3.2.3 Three-point upwind difference scheme

$$a \left[\frac{\partial f}{\partial h} \right]_l = \begin{cases} a \frac{3f_l - 4f_{l-1} + f_{l-2}}{\Delta h} & \text{if } a \geq 0 \\ a \frac{-f_{l+2} + 4f_{l+1} - 3f_l}{\Delta h} & \text{if } a < 0 \end{cases}$$

3.3. Truncation errors

The truncation errors are worthy of some discussions to estimate the accuracy of numerical solutions. The estimates are obtained by Taylor series analysis. The solutions of each scheme of the difference equation of energy are equivalent to the solutions of the following differential equations.

3.3.1 Tow-point upwind difference scheme

$$\begin{aligned} \frac{\partial \bar{\theta}}{\partial t} + \bar{u} \frac{\partial \bar{\theta}}{\partial x} + \bar{v} \frac{\partial \bar{\theta}}{\partial y} &= \left\{ \left(\frac{\lambda_{\theta}}{\bar{\rho} c_p} + K \right) + \Delta x \frac{|\bar{u}|}{2} \right\} \frac{\partial^2 \bar{\theta}}{\partial x^2} \\ &+ \left\{ \left(\frac{\lambda_{\theta}}{\bar{\rho} c_p} + K \right) + \Delta y \frac{|\bar{v}|}{2} \right\} \frac{\partial^2 \bar{\theta}}{\partial y^2} + \left\{ 2 \frac{K}{\bar{\rho}} \frac{\partial \bar{\rho}}{\partial x} + \frac{\partial K}{\partial x} \right\} \frac{\partial \bar{\theta}}{\partial x} \\ &+ \left\{ 2 \frac{K}{\bar{\rho}} \frac{\partial \bar{\rho}}{\partial y} + \frac{\partial K}{\partial y} \right\} \frac{\partial \bar{\theta}}{\partial y} + O(\Delta t) + O(\Delta x^2) + O(\Delta y^2) \end{aligned}$$

as $\Delta t, \Delta x, \Delta y \rightarrow 0$

3.3.2 Central and Three-point upwind difference scheme

$$\begin{aligned} \frac{\partial \bar{\theta}}{\partial t} + \bar{u} \frac{\partial \bar{\theta}}{\partial x} + \bar{v} \frac{\partial \bar{\theta}}{\partial y} &= \left(\frac{\lambda_{\theta}}{\bar{\rho} c_p} + K \right) \frac{\partial^2 \bar{\theta}}{\partial x^2} + \left(\frac{\lambda_{\theta}}{\bar{\rho} c_p} + K \right) \frac{\partial^2 \bar{\theta}}{\partial y^2} \\ &+ \left\{ 2 \frac{K}{\bar{\rho}} \frac{\partial \bar{\rho}}{\partial x} + \frac{\partial K}{\partial x} \right\} \frac{\partial \bar{\theta}}{\partial x} + \left\{ 2 \frac{K}{\bar{\rho}} \frac{\partial \bar{\rho}}{\partial y} + \frac{\partial K}{\partial y} \right\} \frac{\partial \bar{\theta}}{\partial y} \\ &+ O(\Delta t) + O(\Delta x^2) + O(\Delta y^2) \end{aligned}$$

as $\Delta t, \Delta x, \Delta y \rightarrow 0$

The coefficient of the terms $O(\Delta t)$, $O(\Delta x^2)$ and $O(\Delta y^2)$ involves the derivations of high order than it appears in these equations. The truncation errors are evaluated by $O(\Delta t) + O(\Delta x^2) + O(\Delta y^2)$. As the differencing of the convection terms are applied to two-point upwind difference scheme, the diffusion terms are made additions to $\Delta x \frac{|\bar{u}|}{2}$ and $\Delta y \frac{|\bar{v}|}{2}$ which are called numerical viscosity. Using the other difference scheme, however, the numerical viscosity does not come out. Therefore the accuracy of the numerical solutions depends only upon the time and space mesh sizes under no existence of rounding-off errors by numerical computations.

3.4. Practical stability and spurious oscillation

The integration of the parabolic partial differential energy equation in time and space requires the practical stability for the finite difference method. Practical stability imposed restrictions on the size of time mesh and space meshes for the finite difference scheme, but the sizes of Δt , Δx and Δy are arbitrarily given. We obtained the practical stability conditions [5] impose restrictions for each scheme on the mesh sizes of Δt , Δx and Δy as shown in Table 1.

Table 1. The practical stability condition

Numerical scheme	Explicit method	Implicit method
Central	$\Delta t \leq \left[\max_{ijn} \left\{ 2\sigma_{ij}^n \left(\frac{1}{\Delta x^2} + \frac{1}{\Delta y^2} \right) \right\} \right]^{-1}$ $\Delta x \leq \max_{ijn} \frac{2\sigma_{ij}^n}{\bar{u}_{ij}^n} \quad \text{and} \quad \Delta y \leq \max_{ijn} \frac{2\sigma_{ij}^n}{\bar{v}_{ij}^n}$	stable
2-point upward	$\Delta t \leq \left[\max_{ijn} \left\{ \frac{\bar{u}_{ij}^n}{\Delta x} + \frac{\bar{v}_{ij}^n}{\Delta y} + \frac{2\sigma_{ij}^n}{\Delta x^2} + \frac{2\sigma_{ij}^n}{\Delta y^2} \right\} \right]^{-1}$	stable
3-point upward	unstable	stable

We consider the accuracy of computational results for high Reynolds number because of turbulent fluid flow. The computational results have the spurious error [6] under the condition of the effective maximum cell Reynolds number (Re^*) greater than 2 for the equation of motion and the effective maximum cell Peclet number (Pe^*) greater than 2 for the equation of energy because of discretizing the central difference scheme in FDM (Finite Difference Method). However as the diffusion coefficient for the two-point upwind scheme is added to the numerical viscosity, the spurious oscillation is repressed or decreased by numerical viscosity for large value of velocity. Pe^* is defined as follows;

$$Pe^* = \max \left\{ \max_{ijk} \frac{|u_{ij}^n| \Delta x}{\sigma_{ij}^n + K_{ij}^n}, \max_{ijk} \frac{|u_{ij}^n| \Delta y}{\sigma_{ij}^n + K_{ij}^n} \right\}$$

4. Numerical Experiments

We consider the transient natural convection in a fire compartment of two-dimensional rectangular room (2.4 m height and 2.4 m length). Steady flat plate heat source (800°C) is placed [A] at the center of the floor (10 cm width) in Fig. 1 and [B] at the left hand side wall (2.4 m length) in Fig. 2. The fluid in the fire compartment is initially motionless and at a uniform temperature of 30°C. Initial pressure and density distribution are obtained by computation of the equation of state. The ceiling, floor and left side wall are the solid boundary and the right side is the free space boundary. The solid boundaries are assumed to be thermally adiabatic, Neumann type, except to the heating plate and the velocity on the solid boundary is assumed to be Dirichlet type non-slip condition. The boundary conditions on the free space boundary are assumed to be Neumann type condition for out-flow and Dirichlet type condition for in-flow. The simultaneous equations introduced by the implicit difference scheme are solved numerically by the sparse line successive over-relaxation method (SLSOR) for Poisson type equation and two-point upwind difference scheme, and by the sparse conjugate residual II method (SCR2) for other difference scheme to reduce the computer memories of data area. Several numerical experiments were carried out on super computer with FORTRAN 77 used to double precision as follows:

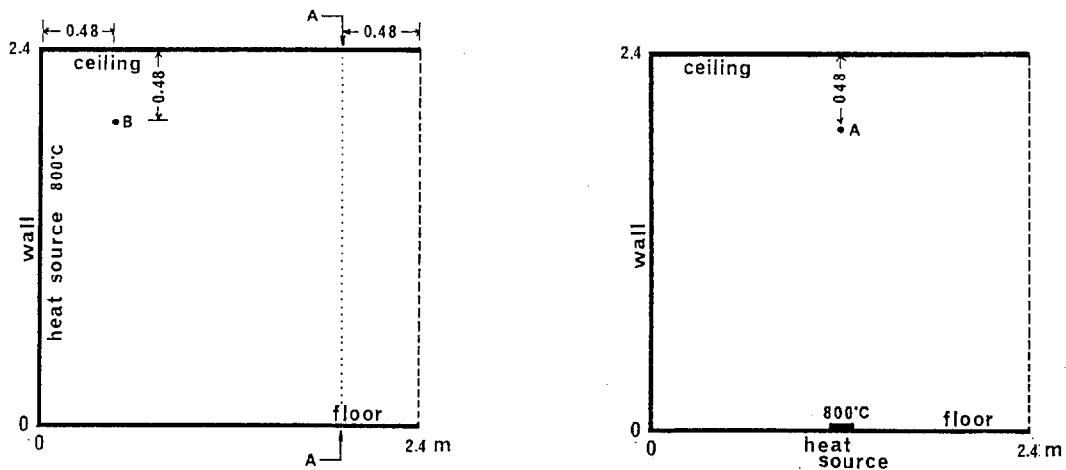


Figure 1. Outline of computational domain Figure 2. Outline of computational domain

4.1. Estimate of the computational results with space mesh

The constant line heat source (800°C and 2.4 m width) is located on the left side solid wall in Fig. 1. The computational domain is subdivided with the total 11×11, 16×16, 21×21, 31×31, 41×41 and 61×61 meshes corresponding to 24, 16, 12, 8, 6, and 4 cm mesh sizes respectively. The temperature, the velocity \bar{u} and \bar{v} of computational results at the location B (48 cm below ceiling and 48 cm far from heat source) and the cross section A (48 cm far from open area on free boundary) in Fig. 1 were compared each space mesh.

4.2. Estimate of the computational results with different finite difference scheme for convection terms

For save charge computing time, the numerical computations were carried out with space mesh size 12 cm and time interval 10 msec in which the heat source is located on the left side solid wall and on the floor in cases of Fig. 1. The scheme for convection term is proposed numerically.

4.3. Estimate of the computational results with time interval

As the results of the estimate of the space mesh, the computational domain is subdivided into 41×41 grids corresponding to 6 cm mesh size in Fig. 2. The computations were carried out with time intervals which are chosen 2.5, 5, 7.5, 10, 15, 20, 30 and 40 msec considering truncation errors. The temperature, the velocity \bar{u} and \bar{v} of computational results at the location A (center of ceiling and 48 cm below ceiling) and the cross section on the free boundary in Fig. 2 were compared.

5. Results and Discussions

5.1. Estimate of the computational results with space mesh

In order to estimate the accuracy of computational results applied to two-point upwind difference, the space meshes are chosen 24, 16, 12, 8, 6 and 4 cm, and the time interval is fixed constant 10 msec. Fig. 3 shows the computational results of the temperature and the velocity \bar{u} at the location B. The temperature differences and the velocity component \bar{u} differences among the space meshes 4, 6 and 8 cm in Fig. 3-a and 3-b respectively are the much same values (less than 5% errors). In Fig. 3-a, the computational results show the oscillation called "spurious oscillation".

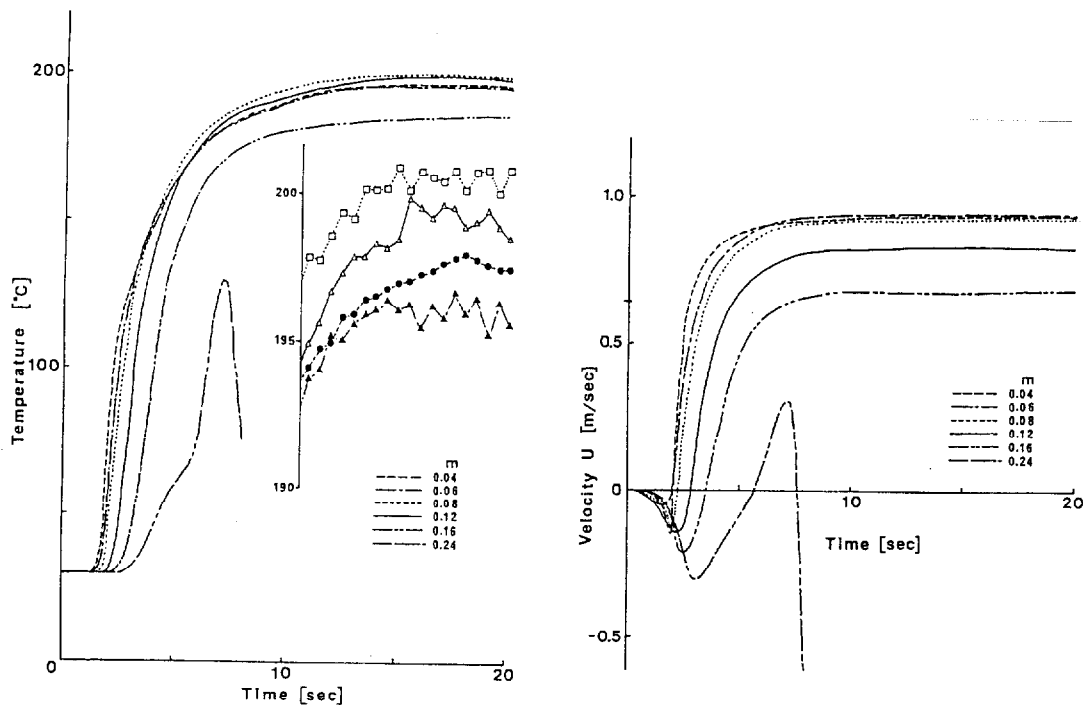


Figure 3. Computational results at the location B in Fig. 1
(a) Temperature and (b) Velocity u

Fig. 4 shows the relationship between Re^* from the computational results and time. This Re^* of 4 cm mesh in Fig. 4 gives the smallest values less than 10 after 10 sec, so the period of spurious oscillation would give the large and the amplitude would give the small. Before 10 sec the flow motion is numerically unstable because of initially putting the constant line heat source temperature 800°C , so the numerical computation with 24 cm mesh and 10 msec time interval was diverged and in the case of 2 cm and 10 msec time interval was also diverged because the simultaneous equations for implicit method were unstable to be solve numerically by the truncation errors and rounding-off errors.

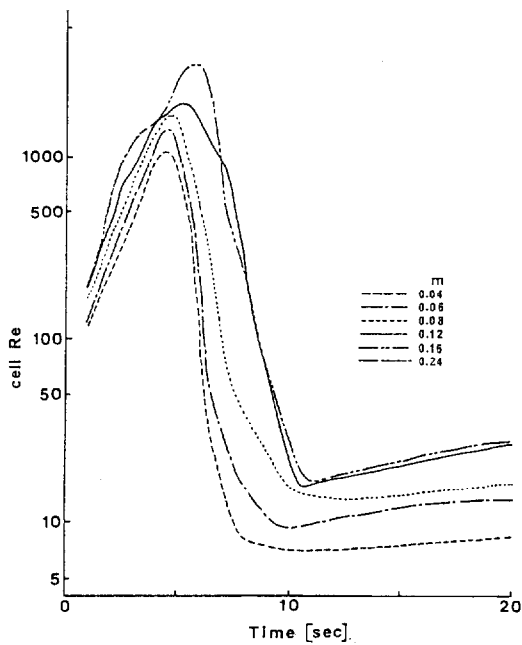


Figure 4. Relationship between Re^* and time

Fig. 5 shows the computational results of the temperature at the cross section A. The results with space mesh sizes 6 and 4 cm are the much same and the other mesh sizes are quite different from them. On the other hand Fig. 6 shows the temperature distribution at the cross section A with time intervals 10 and 5 msec in the case of space mesh 6 cm, and with time intervals 10 msec, 5 msec and 2.5 msec in the case of 4 cm. These time intervals are given by considering truncation errors. As the results the temperature difference is about 10% errors each other.

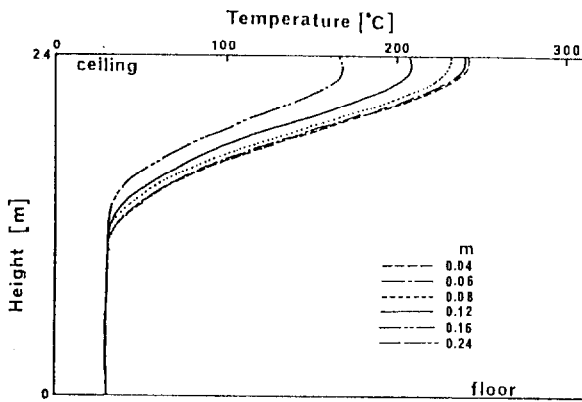


Figure 5. Computational results of temperature at the cross section in Fig. 1.

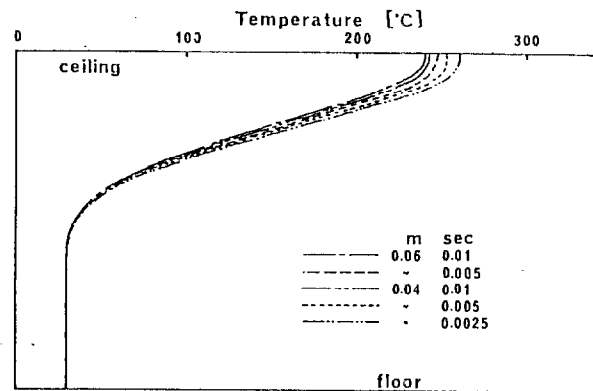


Figure 6. Computational results of temperature at the cross section in Fig. 1.

Table 2 shows the computational run time (CPU time) of 20 simulation seconds.

Table 2. CPU time ratio

Mesh size (cm)	Time interval (msec)		
	10.0	5.0	2.5
16	0.073	—	—
12	0.147	—	—
8	0.418	—	—
6	1.000	1.346	—
4	5.412	7.360	11.419

5.2. Estimate of the computational results with different finite difference scheme for convection terms

Fig. 7 shows the distributions of temperature with the different scheme for convection term in the case of 10 msec time interval and 12 cm mesh at the cross section of free boundary in Fig. 1. As the results the two-point upwind scheme is only quite differences among other scheme, that is, it gives under estimate because of adding the numerical viscosity. Table 3 shows the CPU time until 20 simulation seconds. In above mentions the three-point upwind difference scheme for convection term applied implicit method would be better way.

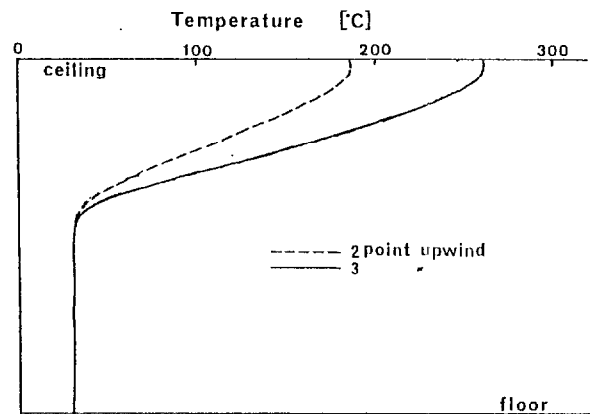


Figure 7. Computational results of temperature at the cross section of free boundary in Fig 1.

5.3. Estimate of the computational results with time interval

The computations were carried out for the accuracy of time interval with 6 cm mesh applied to three-point upwind scheme in the case of Fig. 2. The time intervals are chosen 2.5, 5, 7.5, 10, 15, 20, 30, and 40 msec. In the case of 40 msec time interval the computation miscarried due to numerical errors. It should be noted that the computations were only success the time intervals 7.5, 10, and 15 msec by three-point upwind difference scheme. Fig. 8 shows the temperature and the velocity \bar{u} at the location A.

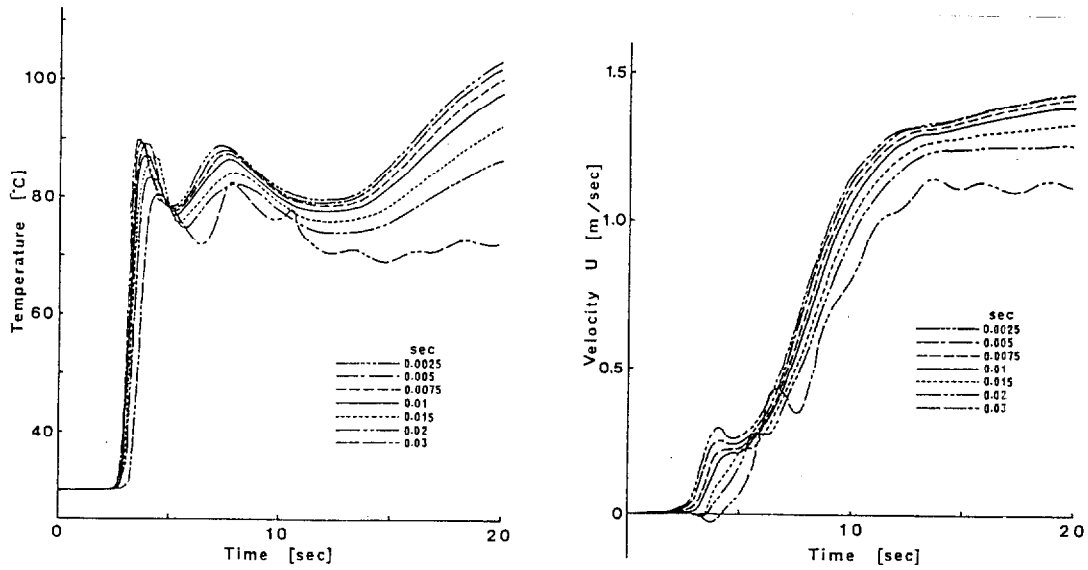


Figure 8. Computational results at the location A in Fig. 2
(a) Temperature and (b) Velocity u

Fig. 9 shows the temperature distributions at the cross section of free boundary. In these figures the results of temperature with 10 msec to 2.5 msec time intervals give about 5% errors each other. The results of the time interval 10 msec come to a full application of its values from above mentions.

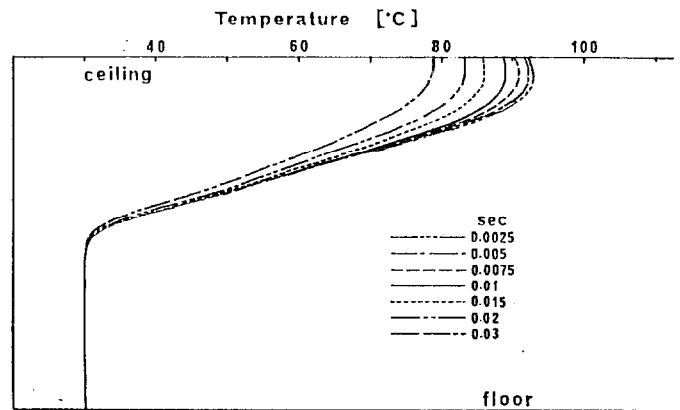


Figure 9. Computational results of temperature at the cross section of free boundary in Fig 2.

6. Conclusion

When the implicit method is used in field model simulations of a compartment fire, our personal point of view from computational experiments is that the time interval and space mesh should be chosen less than 10 msec and 5 cm for high Re and the difference scheme for the convection term should be the three-point upwind difference scheme. The better way is to take $O(\Delta t) \simeq O(\Delta x^2) \simeq O(\Delta y^2)$ and small increment. The mesh sizes, time and space, influence the accuracy from truncation errors under the condition of no rounding-off errors, and the scheme avoids errors due to numerical viscosity. They can be

observed the trust in numerical results by Re^* for the equation of motion and Pe^* for the equation of energy. $Re^* < 20 \sim 30$ or $Pe^* < 20 \sim 30$ could be accepted from numerical experiments.

7. References

- [1] J.E. Fromm & J.J. Smolderen; Numerical Solution of the Navier-Stokes Equation at High Reynolds Number and the Problem of Discretization of Convective Derivatives; Numerical Methods in Fluid Dynamics; AGARD Lecture Series, No. 48 (1972)
- [2] O.A. Ladyzhenskaya; The Mathematical Theory of Viscous Incompressible Flow; Gordon and Beach (1969)
- [3] Y. Hasemi; Numerical Simulation of the Natural Convection in Fire Compartment; 2nd Joint Meeting UJNR (1976)
- [4] Richtmyer & Morton; Difference Methods for Initial Value Problems; John Wiley & Sons (1967)
- [5] M. Morita et.al; Feasibility of Numerical Computational Methods of Heat Flow in Fire Compartment; 2nd International Symposium of IAFSS (1988)
- [6] S. Ono & K. Hane; Advances in Numerical Method for Larger Sparse Set of Linear Equation No. 2 (1986)